Topological classification for intersection singularities of exceptional surfaces in pseudo-Hermitian systems

Hongwei Jia[1,2,#], Ruo-Yang Zhang[1,#], Jing Hu[1], Yixin Xiao[1], Yifei Zhu[3,*], C. T. Chan[1,2,†]

[1]Department of Physics, the Hong Kong University of Science and Technology, Clear Water Bay, Kowloon, Hong Kong, China

[2]Institute for Advanced Study, the Hong Kong University of Science and Technology, Clear Water Bay, Kowloon, Hong Kong, China

[3]Department of Mathematics, Southern University of Science and Technology, Shenzhen, Guangdong, China

#These authors contributed equally to this work

*zhuyf@sustech.edu.cn; †phchan@ust.hk

Abstract: Exceptional points play a pivotal role in the topology of non-Hermitian systems, and significant advances have been made in classifying exceptional points and exploring the associated phenomena. Exceptional surfaces, which are hypersurfaces of exceptional degeneracies in parameter space, can support hypersurface singularities, such as cusps, intersections and swallowtail catastrophes. Here we topologically classify the intersection singularity of exceptional surfaces for a generic pseudo-Hermitian system with parity-time symmetry. By constructing the quotient space under equivalence relations of eigenstates, we reveal that the topology of such gapless structures can be described by a non-Abelian free group on three generators. Importantly, the classification predicts a new kind of non-Hermitian gapless topological phase and can systematically explain how the exceptional surfaces and their intersections evolve under perturbations with symmetries preserved. Our work opens a new pathway for designing systems with robust topological phases, and provides inspiration for applications such as sensing and lasing which can utilize the special properties inherent in exceptional surfaces and intersections.

Introduction. Singularities, characterized by the property of non-differentiability, are ubiquitous and play important roles in many physical systems in the real world. The occurrence of a singularity is usually accompanied by exotic physical phenomena [1,2,3,4,5,6,7,8,9,10,11,12,13]. In topological materials, a Weyl point in a Hermitian system acts as a sink or source of the Berry curvature, and two Weyl points with opposite chiralities are connected by a Fermi-arc surface state [1,2,9,11]. Topology is pivotal in understanding the existence and stability of singularities, and a singularity can be characterized by a topological invariant (e.g. Chern number), which is usually encoded in the adiabatic evolution of eigenstates on closed loops/surfaces enclosing it [5,6,7,8,9,11]. Recently, the topology of non-Hermitian systems is attracting growing attention [14,15,16,17,18,19,20,21,22,23,24,25]. Non-Hermiticity is ubiquitous because most systems are not isolated where the eigen-energies become complex numbers, representing energy exchange with surrounding environment. The exceptional points, as a unique feature of non-Hermiticity, are singular points on the complex energy plane where both the eigenenergies and the eigenstates coalesce [14,15,16,18,19]. Different from Hermitian degeneracies such as Weyl points and nodal lines, the exceptional point may carry fractional topological invariants [16,18,19,24,26], and can induce stable bulk Fermi-arcs [22,24] and braiding of eigenvalues [26]. The non-Hermitian skin effect, manifested by the strong dependence of the eigen-spectrum on boundary conditions, is associated with the point gaps in bulk topology [15,16,17,18,21,23,25]. Recent discoveries of lines, rings and surfaces of exceptional points further enriched the classes of topological degeneracies [27,28,29,30,31]. High-order exceptional degeneracies, which often appear as cusps of exceptional lines/surfaces, carry hybrid topological invariants in a higher dimensional parameter space [32].

Lots of efforts have been devoted to classifying exceptional points recently. Topological classifications are important, because whenever the type of energy gaps and Altland-Zirnbauer symmetry class for the system are known, the degeneracies in the parameter space are predictable [14,19,20,33,34,35]. It is thus a theoretical framework for predicting non-Hermitian topological phases of matter, providing guidance for experimental realizations. Particularly, exceptional points can

assemble into hypersurfaces in 3D parameter space, dubbed exceptional surfaces (ESs), separating exact and broken phases [20]. The ES are commonly observed in non-Hermitian systems with parity-time inversion symmetry (*PT*) or chiral symmetry [20,27,28,29], and have broad applications in the design of sensing and absorption devices [31,36]. As a subspace of the parameter space, ESs may possess embedded sub-dimensional singularities, the so-called hypersurface singularities, that have remarkable properties differentiating them from other points on the ESs, such as intersections [37], cusps [38,39,40], and swallowtail catastrophes [41]. Such hypersurface singularities are symmetry protected [31,37,38,39,40,41], and are stable against perturbations with symmetries preserved. However, despite various important physical phenomena and potential applications, the hypersurface singularities on ESs were never topologically classified.

The non-defective intersection line (NIL) of ESs should be the simplest form of hypersurface singularities, which is an elementary singular line composing the swallowtail catastrophe [41]. In this work, we consider a generic two-level non-Hermitian system, which preserves *PT* symmetry plus an additional pseudo-Hermitian symmetry. The band structures of such systems exhibit non-defective intersection lines (NIL) of ESs. By analyzing equivalence relations of eigenstates, we discover that the quotient space of the order-parameter space is homotopy equivalent to a bouquet of three circles $M = S^1 \vee S^1 \vee S^1$. The topology of the NIL is thus represented by the fundamental group of *M*, which is a non-Abelian free group on three generators. The topological charges represented by the group elements can be associated with frame deformation of eigenstates. Besides, the conservation of topological charges is manifested by the robustness of ESs and NILs against perturbations to the Hamiltonian.

Main. The prototypical Hamiltonian is a two-level system, which is *PT* symmetric and also preserves an additional η-pseudo-Hermitian symmetry [41,42,43]

$$[H, PT] = 0, \qquad \eta H \eta^{-1} = H^{\dagger} \tag{1}$$

The *PT* operator can be regarded as complex conjugation with a proper choice of basis in parameter space, and thus the Hamiltonian can always be gauged to be real. The metric operator η here takes the

Minkowski metric $\eta = \mathrm{diag}(-1,1)$ [13,41,44,45]. It is notable that in case the Hamiltonian performs unitary transformations, η transforms simultaneously (see Section 1 in [46] for details). These symmetries imply that the momentum space Hamiltonian can be written in the form

$$H(\mathbf{k}) = f_2(\mathbf{k})i\sigma_2 + f_3(\mathbf{k})\sigma_3 \tag{2}$$

where $f_{2,3}$ are real functions in three-dimensional (3D) **k**-space, and $\sigma_{2,3}$ are Pauli matrices. The term multiplied by an identity matrix can be ignored because it has no impact on the gapless structure. Such Hamiltonians correspond to physical systems with non-reciprocal hopping [41,47,48,49] of orbitals.

The 2D f_2-f_3 plane is exactly the order parameter space of all the Hamiltonians preserving the symmetries in Eq. (1) due to the following reasons: Any ESs in 3D **k**-space can be mapped to the exceptional lines (ELs) at $f_2 = \pm f_3$, and these surface intersections (NILs) correspond to the intersecting point (NIP) of the two ELs at the origin $f_2 = f_3 = 0$; a path in **k**-space can be mapped to a path on the f_2-f_3 plane, and if the path circulates around the NIL, the corresponding path on f_2-f_3 plane circulates around the NIP. The gapless structure of the order parameter space is shown in Fig. 1a, with the red and green lines denoting EL_1 and EL_2 satisfying $f_2 = \mp f_3$, respectively. In regions I and III (satisfying $|f_2| < |f_3|$), the eigenenergies are real, which are *PT*-exact phases. In contrast, regions II and IV (satisfying $|f_2| > |f_3|$) are *PT*-broken phases, with eigenvalues forming complex-conjugate pairs. The paths α, α', β and β' are terminated at different ELs in parameter space. The NIP at the origin is what we want to classify, and is excluded from the 2D plane [20,50]. Any paths or loops cannot traverse the NIP. First, the 2D plane with a hole at the origin can deformation retract to a circle S^1 [Fig. 1(b)]. Such a mathematical process can be interpreted as a quotient map, which identifies all points on the ray starting from the origin (note that the origin is excluded). As a consequence, all points on upper half of EL_1 shrink to point A, and the lower half shrinks to point A'. Similar process applies to EL_2, with the upper and lower halves shrinking to B and B'. There also exist equivalence relations on the S^1. At point A, the two eigenstates coalesce, which is totally the same as the coalesced state at point A'. Therefore, A and A' can be identified, and we glue A' to A via a quotient map. The same procedure applies to B and

B'. It is notable that antipodal points lying in the gap cannot be identified. The essential difference is that each of these points has two linearly independent eigenstates, and the two eigenstates are ordered by the corresponding eigenenergies. The sequence of eigenenergies in exact phases (Regions I and III) is well-defined. In broken phases, the real parts of eigenenergies coalesce, and we simply order the eigenstates by the imaginary parts of eigenenergies. One can either sort the imaginary parts from negative to positive or from positive to negative, and the only requirement is that the criterion in Regions II and IV of broken phases should be unified. Consequently, even though a pair of antipodal points in the gap have the same eigenstates, but the eigenstates are ordered inversely for the two points based on the eigenenergies, which thus cannot be identified. With the above procedures, we obtain the quotient space (details of quotient space are shown in Section 2 of [46]) of the S^1 in Fig. 1(b), which is a bouquet of three circles [see Fig. 1(c)],

$$M = S^1 \vee S^1 \vee S^1 \tag{3}$$

The fundamental group of M can thus be derived as

$$\pi_1(M) = \mathbf{Z} * \mathbf{Z} * \mathbf{Z} \tag{4}$$

which is a free non-Abelian group on three generators. As indicated by Fig. 1(c), the generators Z_1, Z_2 and Z_3 can be characterized by the paths combinations $\alpha\beta$, $\alpha\alpha'^{-1}$ and $\alpha'\beta'$, respectively. These topological invariants can be assocated with the frame deformations of eigenstates, details are shown in [46].

We next introduce some typical trivial and nontrivial loops (or combined paths) in parameter space to better understand the group [Eq. (4)]. The combined paths characterizing the generators Z_1, Z_2 and Z_3 are shown in Fig. 2(a-c), respectively, where the dashed lines with arrows denote quotient maps that glue identified points. We note that the gluing process does not mean the loop traverses the NIP. Each of the combined paths corresponds to an S^1 in Fig. 1c, which are exactly closed loops in quotient space M. *A closed loop encircling the NIP is also a path combination $\alpha\beta\alpha'\beta'$, which characterizes the topological invaraint Z_1Z_3, being an element in the group [Eq. (4)]. Topologically protected edge states can arise from Z_1Z_3, and details are shown in Section 4 of [46].* Some other nontrivial loops are discussed in Section 5 of [46]. It is found that all nontrivial loops (paths) have to traverse ELs. Any

loop that does not touch ELs is confined in a specific region, e.g. loop l in Fig. 3e, and is always trivial because it cannot enclose any singularity. As we move the loop across the EL, l is decomposed into two paths l_1 and l_2 (Fig. 3f). As the terminal points of l_1 (or l_2) can be identified, l_1 (or l_2) is also a loop in quotient space M, but is a trivial loop that can shrink to a point. Therefore, the combination $l_1 l_2$ is also trivial. By stretching the loop to cross the other EL (see Fig. 3g), l becomes a composite of $l_1 l_3 l_4 l_5$. Since both l_1 and l_4 correspond trivial loops in quotient space M, the composite is equivalent to the combination $l_3 l_5$. In addition, paths l_3 and l_5 are along opposite directions and are homotopic to α^{-1} and α, respectively. It is thus not difficult to find out that the combination $l_1 l_3 l_4 l_5$ remains trivial. *From this analysis, we can conclude that a loop (or a path) encountering ELs through continuous deformations will not change the topology. In contrast, encountering NIPs is not allowed, which will change the topology.* Similar discussion can also be found in [41]. These results indicate that the NIP, as a hypersurface singularity, is distinguished from isolated singularities. An open path for an isolated singularity is meaningless because it cannot enclose the singularity. Conversely, a path joining ELs (or ESs) can provide a lot of information on the NIP (see more details in Section 3 of [46]). Therefore, if a loop is partitioned into several segments by ELs (or ESs), it is necessary to investigate the evolution of eigenstates on each path and then discuss the combinations. Since the non-trivial loops all traverse the hypersurfaces, our method is affiliated to intersection homotopy theory [50,51].

With these elementary invariants taken from the group, we are able to predict how singularities evolve under the constraint of topological invariants as the Hamiltonian deforms. We are more interested in the 3D **k**-space, in which the NILs and ESs correspond to NIP and ELs on the f_2-f_3 plane, respectively. Consider the following example

$$f_2(\mathbf{k}) = k_x k_z, \quad f_3(\mathbf{k}) = -k_x^2 + k_y^2 + k_z^2 - d \qquad , \tag{5}$$

for which the chain of NILs and ESs in 3D **k**-space for d=1 are shown in Fig. 3a1, where the red and green surfaces denoted by ES_1 and ES_2 satisfying $f_2 = \mp f_3$ and corresponds to EL_1 and EL_2 (Fig. 1), respectively. We first look at the loop l_6 in Fig. 3a1, which encloses the waists of two ESs and their intersections NILs (satisfy $f_2 = f_3 = 0$), but does not touch any ESs. Such a loop is trivial according to

our previous conclusion, which is not obvious in the figure because these ESs and NILs seemingly prevent the loop from retracting to a point. However, by changing d from positive to negative, the waists of ESs and NIL gradually retract to a point (Fig. 3b1), and finally open up to form a bandgap (Fig. 3c1). The two NILs enclosed by the loop are thus annihilable. This is a solid evidence that l_6 is a trivial loop. The trivial loop l_6 enforces the ESs connecting the two NILs to remain smooth as the Hamiltonian deforms. This can be explained by l_6' (see Fig. 3a1), which is equivalent to l_6, as they enclose the same NILs, but traverses ESs. On the section plane that l_6' lying on, l_6' is segmented by ESs into several paths, as sketched in Fig. 3a2, where the red and green lines denote the ESs cut by the plane. The invariants on the segments of l_6' must cancel each other to form a trivial product, implying that the path l_t is trivial, which can be directly seen from the fact that the path l_t is a trivial path with both ends on a smooth ES (see Fig. 3a2). As one continues to deform the Hamiltonian, the two ESs enclosed become disconnected after the two NILs annihilate (see Fig. 3c1-c2). Now we turn to l_7 in Fig. 3a1, which is segmented by the ESs into different paths, as indicated by Fig. 3a3. The loop is a path combination $(\beta^{-1}\alpha^{-1}\beta'^{-1}\alpha'^{-1})^2$, carrying a squared topological invariant $(Z_1^{-1}Z_3^{-1})^2$. This nontrivial invariant forbids the two encircled NILs to annihilate as d varies in the Hamiltonian (Eq. 5). The two NILs merge at a point for d=0 (Fig. 3b1), and the nearby area is partitioned into eight regions (see Fig. 3b3), meaning that the point still carries the squared invariant $(Z_1^{-1}Z_3^{-1})^2$. As one keeps varying d, the point splits, and the two NILs become separate in the other direction, as shown in Fig. 3c1 and c3. The squared invariant $(Z_1^{-1}Z_3^{-1})^2$ is conserved within the deformation process of the Hamiltonian. *We thus understand that the squared invariant $(Z_1^{-1}Z_3^{-1})^2$ is a necessary condition for the chain of NILs.* Another condition for the presence of the chain of NILs is the mirror symmetries $k_x \rightarrow -k_x$ and $k_z \rightarrow -k_z$, which will be illustrated in a tight binding model to be described below. The conservation of the invariant also shows that two inannihilable NILs cannot be directly connected by smooth ESs, as can be observed in Fig. 3a3-c3.

Non-reciprocal tight binding model. The model Hamiltonian can be realized in real space using a tight binding model with non-reciprocal hoppings. A 3D fcc lattice model and the corresponding Brillouin

zone are shown in Fig. 4a-b, where M and N denote two inequivalent lattice sites with opposite onsite energies $\pm E_0$. The hopping between M and N (on dark green bonds) is non-reciprocal ($M\rightarrow N$: t_1, $M\rightarrow N$: $-t_1$), and the hoppings on yellow and red bonds [between the adjacent sites in the same sublattice but in different directions, i.e. yellow bonds: $\vec{r}_M \rightarrow \vec{r}_M + \vec{a} + \vec{b}$ and $\vec{r}_N \rightarrow \vec{r}_N + \vec{a} - \vec{b}$; red bonds: $\vec{r}_M \rightarrow \vec{r}_M + \vec{a} - \vec{b}$ and $\vec{r}_N \rightarrow \vec{r}_N + \vec{a} + \vec{b}$] are characterized by t_2 and $-t_2$, respectively. The corresponding real space Hamiltonian is given by

$$\begin{aligned} H_1 = & \sum_{\substack{\vec{r}_M \in \vec{G}_M \\ \vec{\alpha}=\vec{a},\vec{b},\vec{c}}} t_1 (a^\dagger_{M,\vec{r}_M} a_{N,\vec{r}_M+\vec{\alpha}} + a^\dagger_{M,\vec{r}_M} a_{N,\vec{r}_M-\vec{\alpha}}) - h.c. + E_0 (a^\dagger_{M,\vec{r}_M} a_{M,\vec{r}_M} - a^\dagger_{N,\vec{r}_N} a_{N,\vec{r}_N}) \\ & + \sum_{\substack{\vec{r}_h \in \vec{G}_h \\ h=M,N}} \mathrm{sgn}(h) t_2 (a^\dagger_{h,\vec{r}_h} a_{h,\vec{r}_h+\vec{a}+\vec{b}} + h.c. - a^\dagger_{h,\vec{r}_h} a_{h,\vec{r}_h+\vec{a}-\vec{b}} - h.c.) \end{aligned} \tag{6}$$

where $\vec{a}$, $\vec{b}$ and $\vec{c}$ are the set of orthogonal lattice vectors connecting lattice sites M and N (see Fig. 4a). Here sgn(h)=1 and –1 for h=M and N, respectively. The corresponding **k**-space Hamiltonian (see details in Section 6 of [46]) shows that $f_3(\mathbf{k}) = E_0 + 2\sin k_x \sin k_y$ and $f_2(\mathbf{k}) = \cos k_x + \cos k_y + \cos k_z$. The system has mirror symmetries in the x and y directions for E_0=0, and thus the band structure is symmetric about k_x=π/d_L and k_x=0 planes. The ESs and NILs for E_0=0 are plotted in Fig. 4c, where the red and green surfaces are ESs satisfying $f_2 = \mp f_3$, respectively As can be seen, a chain of NILs is formed on the intersection line of the k_x=π/d_L and k_y=0 planes (see Fig. 4c). The orange dashed loop (Fig. 4d) is a combination $(\alpha'\beta'\alpha\beta)^2$ that carries a squared topological invariant $(Z_3Z_1)^2$. The blue dashed loop does not traverse any ES and is trivial. The mirror symmetries and the topological invariants on the two loops ensure the presence of intersection points of NILs (red arrows). A nonzero E_0 can break the mirror symmetries in k_x and k_y directions, which eliminates the intersection points (as shown in Fig. 4e). However, the breaking of mirror symmetries does not affect the topology on the loops. As shown in Fig. 4e, the blue loop is still trivial, because it does not touch any ESs. The topological invariant on the orange loop is conserved [still $(Z_3Z_1)^2$], as the traversed ESs remain the same (Fig. 4d and 4f). The variation of ESs and NILs with respect to perturbations to the Hamiltonian is thus predictable in view of the conservation of topological charges.

In summary, we topologically classified a generic non-Hermitian two-level system with *PT* and an additional pseudo-Hermitian symmetries, which can be realized in systems with non-reciprocal hoppings [41,47,48,49]. Such systems exhibit surfaces of exceptional points, which intersect stably in momentum space. We showed that the topology of such gapless structure can be understood from the quotient space under equivalence relations of eigenstates, which is a bouquet of three circles. Its fundamental group is isomorphic to a free non-Abelian group on three generators. The group structure allows the prediction of the evolution of ESs and NILs as the Hamiltonian deforms. The method of quotient space topology might potentially be extended to classify other hypersurface singularities in non-Hermitian systems, such as high-order exceptional points as cusps [32,40] and more complicated swallowtail catastrophes [41]. Our work predicts a new kind of non-Hermitian gapless topological phase of matter, providing pathways for designing systems to realize robust topological non-defective degeneracies in non-Hermitian systems. Future theoretical and experimental works on investigating the bulk-edge correspondence for hypersurface singularities may stem from this work. The classification also provides guidance for the design of relevant devices in sensing and lasing applications using exceptional surfaces and their intersections.

Acknowledgements: This work is supported by Research Grants Council of Hong Kong through grants AoE/P-502/20, 16307621, 16307821, 16307420, 16310420 and Croucher Foundation (CAS20SC01) and KAUST20SC01. Y. Zhu acknowledges the financial support from National Natural Science Foundation of China (NSFC) grant 11701263.

References:

[1] L. Lu, L. Fu, J. D. Joannopoulos, et al. Weyl points and line nodes in gyroid photonic crystals, Nat. Photon. **7**, 294-299 (2013).

[2] L. Lu, J. D. Joannopoulos, M. Soljačić, Topological photonics, Nat. Photon. **8**, 821-829 (2014).

[3] D. A. Abanin, S. V. Morozov, L. A. Ponomarenko, et al. Giant nonlocality near the Dirac point in graphene, Science **332**, 328-330 (2011).

[4] Z. Jiang, Y. Zhang, H. L. Stormer, et al. Quantum Hall states near the charge-neutral Dirac point in graphene, Phys. Rev. Lett. **99**, 106802 (2007).

[5] L. Lu, Z. Wang, D. Ye, et al. Experimental observation of Weyl points, Science **349**, 622-624 (2015).

[6] Q. S. Wu, A. A. Soluyanov, T. Bzdušek, Non-Abelian band topology in noninteracting metals, Science **365**, 1273-1277 (2019).

[7] E. Yang, B. Yang, O. You, et al. Observation of non-Abelian nodal links in photonics, Phys. Rev. Lett. **125**, 033901 (2020).

[8] Q. Guo, T. Jiang, R. Y. Zhang, et al. Experimental observation of non-Abelian topological charges and edge states, Nature **594**, 195-200 (2021).

[9] A. A. Soluyanov, D. Gresch, Z. Wang, et al. Type-ii weyl semimetals, Nature **527**, 495-498 (2015).

[10] L. X. Yang, Z. K. Liu, Y. Sun, et al. Weyl semimetal phase in the non-centrosymmetric compound TaAs, Nat. Phys. **11**, 728-732 (2015).

[11] B. Yang, Q. Guo, B. Tremain, et al. Ideal Weyl points and helicoid surface states in artificial photonic crystal structures, Science **359**, 1013-1016 (2018).

[12] H. Jia, R. Zhang, W. Gao, et al. Observation of chiral zero mode in inhomogeneous three-dimensional Weyl metamaterials, Science **363**, 148-151 (2019).

[13] H. Jia, R. Y. Zhang, W. Gao, et al. Chiral transport of pseudospinors induced by synthetic gravitational field in photonic Weyl metamaterials, Phys. Rev. B **104**, 045132 (2021).

[14] Z. Gong, Y. Ashida, K. Kawabata, et al. Topological phases of non-Hermitian systems, Phys. Rev. X **8**, 031079 (2018).

[15] S. Yao, Z. Wang, Edge states and topological invariants of non-Hermitian systems, Phys. Rev. Lett. **121**, 086803 (2018).

[16] H. Shen, B. Zhen, L. Fu, Topological band theory for non-Hermitian Hamiltonians, Phys. Rev. Lett. **120**, 146402 (2018).

[17] N. Okuma, K. Kawabata, K. Shiozaki, et al. Topological origin of non-Hermitian skin effects, Phys. Rev. Lett. **124**, 086801 (2020).

[18] D. Leykam, K. Y. Bliokh, C. Huang, et al. Edge modes, degeneracies, and topological numbers in non-Hermitian systems, Phys. Rev. Lett. **118**, 040401 (2017).

[19] E. J. Bergholtz, J. C. Budich, F. K. Kunst, Exceptional topology of non-Hermitian systems, Rev. Mod. Phys. **93**, 015005 (2021).

[20] K. Kawabata, K. Shiozaki, M. Ueda, et al. Symmetry and topology in non-Hermitian physics, Phys. Rev. X **9**, 041015 (2019).

[21] D. S. Borgnia, A. J. Kruchkov, R. J. Slager, Non-Hermitian boundary modes and topology, Phys. Rev. Lett. **124**, 056802 (2020).

[22] K. Kawabata, T. Bessho, M. Sato, Classification of exceptional points and non-Hermitian topological semimetals, Phys. Rev. Lett. **123**, 066405 (2019).

[23] F. Song, S. Yao, Z. Wang, Non-Hermitian topological invariants in real space, Phys. Rev. Lett. **123**, 246801 (2019).

[24] H. Zhou, C. Peng, Y. Yoon, et al. Observation of bulk Fermi arc and polarization half charge from paired exceptional points, Science **359**, 1009-1012 (2018).

[25] T. Helbig, T. Hofmann, S. Imhof, et al. Generalized bulk–boundary correspondence in non-Hermitian topolectrical circuits, Nat. Phys. **16**, 747-750 (2020).

[26] K. Wang, A. Dutt, C. C. Wojcik, et al. Topological complex-energy braiding of non-Hermitian bands, Nature **598**, 59-64 (2021).

[27] Zhou H, Lee J Y, Liu S, et al. Exceptional surfaces in PT-symmetric non-Hermitian photonic systems, Optica **6**, 190-193 (2019).

[28] R. Okugawa, T. Yokoyama, Topological exceptional surfaces in non-Hermitian systems with parity-time and parity-particle-hole symmetries, Phys. Rev. B **99**, 041202 (2019).

[29] X. Zhang, K. Ding, X. Zhou, et al. Experimental observation of an exceptional surface in synthetic dimensions with magnon polaritons. Phys. Rev. Lett. **123**, 237202 (2019).

[30] Z. Yang, J. Hu, Non-Hermitian Hopf-link exceptional line semimetals, Phys. Rev. B **99**, 081102 (2019).

[31] Q. Zhong, J. Ren, M. Khajavikhan, et al. Sensing with exceptional surfaces in order to combine sensitivity with robustness, Phys. Rev. Lett. **122**, 153902 (2019).

[32] W. Tang, X. Jiang, K. Ding, et al. Exceptional nexus with a hybrid topological invariant[J]. Science **370**, 1077-1080 (2020).

[33] C. C. Wojcik, X. Q. Sun, T. Bzdušek, et al. Homotopy characterization of non-Hermitian Hamiltonians, Phys. Rev. B **101**, 205417 (2020).

[34] X. Q. Sun, C. C. Wojcik, S. Fan, et al. Alice strings in non-Hermitian systems, Phys. Rev. Res. **2**, 023226 (2020).

[35] Z. Li, R. S. K. Mong, Homotopical characterization of non-Hermitian band structures, Phys. Rev. B **103**, 155129 (2021).

[36] S. Soleymani, Q. Zhong, M. Mokim, et al. Chiral Coherent Perfect Absorption on Exceptional Surfaces, arXiv preprint arXiv:2107.06019, 2021.

[37] Y. X. Xiao, K. Ding, R. Y. Zhang, et al. Exceptional points make an astroid in non-Hermitian Lieb lattice: Evolution and topological protection, Phys. Rev. B **102**, 245144 (2020).

[38] S. Sayyad, M. Stalhammar, L. Rodland, et al. Symmetry-protected exceptional and nodal points in non-Hermitian systems, arXiv preprint arXiv:2204.13945, 2022.

[39] X. Cui, R. Y. Zhang, W. J. Chen, et al. Symmetry-protected topological exceptional chains in non-Hermitian crystals, arXiv preprint arXiv:2204.08052, 2022.

[40] P. Delplace, T. Yoshida, Y. Hatsugai, Symmetry-protected multifold exceptional points and their topological characterization, Phys. Rev. Lett. **127**, 186602 (2021).

[41] J. Hu, R. Y. Zhang et al. Non-Hermitian swallowtail catastrophe revealing transitions across diverse topological singularities, Research Square preprint [https://doi.org/10.21203/rs.3.rs-1853770/v1] (2022).

[42] A. Mostafazadeh, Pseudo-Hermitian representation of quantum mechanics, Int. J. Geo. Meth. Mod. Phys. **7**, 1191-1306 (2010).

[43] A. Mostafazadeh, Quantum brachistochrone problem and the geometry of the state space in pseudo-Hermitian quantum mechanics, Phys. Rev. Lett. **99**, 130502 (2007).

[44] D. Z. Freedman, A. Van Proeyen, Supergravity, Cambridge university press, 2012.

[45] T. Frankel, The geometry of physics: an introduction, Cambridge university press, 2011.

[46] Supplemental materials

[47] S. Buddhiraju, A. Song, G. T. Papadakis, et al. Nonreciprocal metamaterial obeying time-reversal symmetry, Phys. Rev. Lett. **124**, 257403 (2020).

[48] X. Wang, G. Ptitcyn, V. S. Asadchy, et al. Nonreciprocity in bianisotropic systems with uniform time modulation, Phys. Rev. Lett. **125**, 266102 (2020).

[49] M. Ezawa, Non-Hermitian non-Abelian topological insulators with PT symmetry, Phys. Rev. Res. **3**, 043006 (2021).

[50] E. H. Spanier, Algebraic topology, Springer Science & Business Media, 1989.

[51] P. Gajer, The intersection Dold-Thom theorem, Topology **35**, 939-967 (1996).

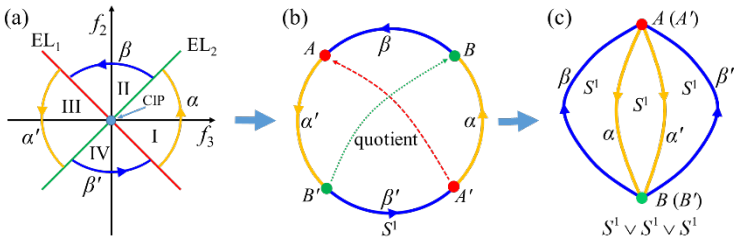

Fig. 1. Construction of quotient space under equivalence relations. (a) The gapless structure of parameter space, $EL_{1,2}$ characterize exceptional lines satisfying $f_2 = \mp f_3$, respectively. The NIP is at the origin. Regions I and III are *PT*-exact phases, and Regions II and IV are *PT*-broken phases. The ELs intersect at f_2=f_3=0. (b) The 2D plane excluding the NIP can deformation retract to a circle S^1, with the upper and lower parts of EL_1 shrinking to A and A', respectively. Similarly upper and lower parts of EL_2 shrink to B and B', respectively. (c) Gluing identified points A with A', and B with B', the quotient space of S^1 in (b) can be obtained as a bouquet of three circles.

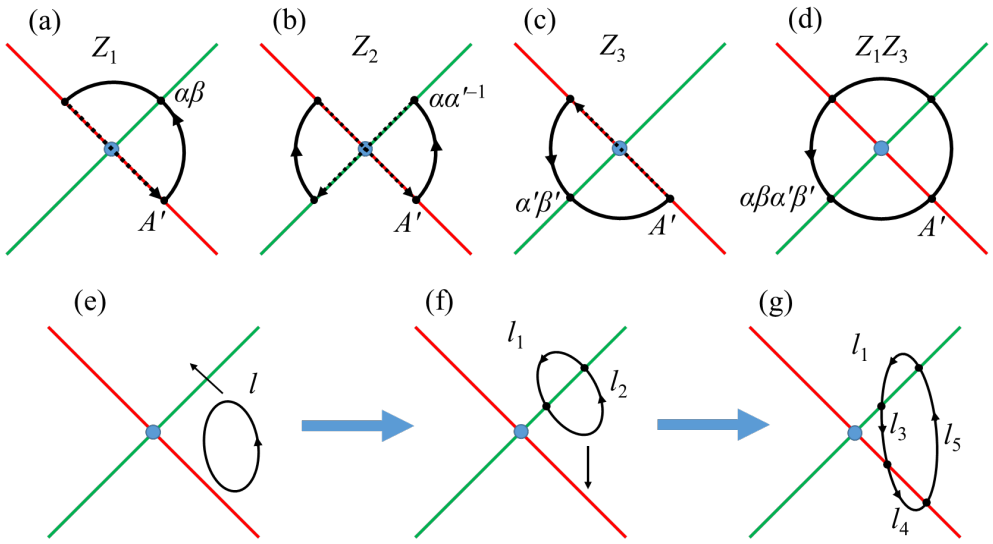

Fig. 2. Typical nontrivial and trivial loops. (a-c) Nontrivial loops characterizing generators Z_1, Z_2 and Z_3, where the dashed lines with arrows denote quotient maps, i.e. gluing identified points. (d) The loop formed by the combination $\alpha\beta\alpha'\beta'$ encloses the NIP, which characterizes the topological invariant Z_1Z_3. Point A' in (a-d) denotes the basepoint. (e) A loop without touching ELs is confined within a specific region and is trivial. (f) Moving the loop along the black arrow direction [see (e)], the loop becomes a composite of paths l_1 and l_2. Both of l_1 and l_2 are trivial, and their composite loop is also trivial. (g) Stretching the loop along the black arrow direction in (f), the loop crosses EL_1 and becomes a composite of paths $l_1l_3l_4l_5$. The path l_4 corresponds to a trivial loop in quotient space M. The paths l_5 and l_3 are in opposite directions, and are homotopic to α and α^{-1}, respectively. The path product $l_1l_3l_4l_5$ is thus trivial.

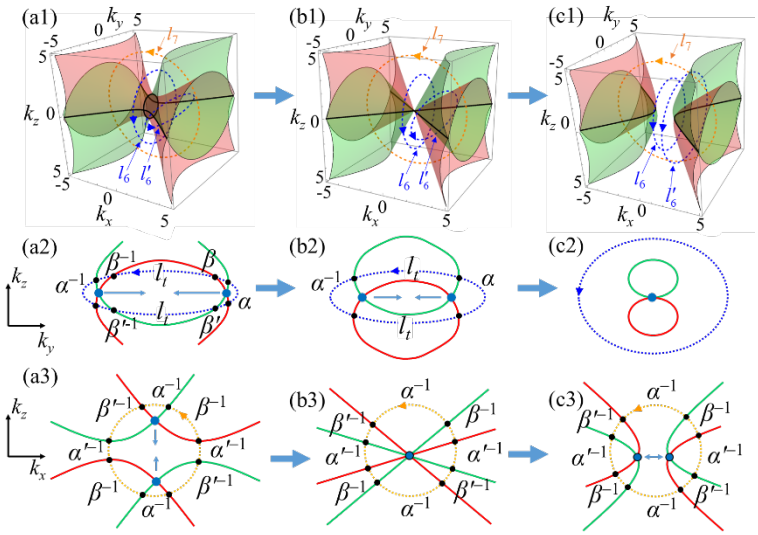

Fig. 3. Evolution of ESs and NILs against perturbations to the Hamiltonian. (a1-c1) ESs (red and green surfaces) and NILs (black lines) plotted with Eq. 5, corresponding to $d > 0$, $d = 0$ and $d < 0$, respectively. The blue loops l_6 and l_6' have trivial topological invariants. (a2-c2) Cross section of the plane that l_6' locates on. The enclosed pair of NILs can annihilate each other. (a3-c3) Cross section of the plane that the orange l_7 locates on. The NILs enclosed cannot annihilate each other. Red and green lines: ESs; Dark blue dots: NILs; Black dots: intersecting points of loops on ESs (in Row 2 and Row 3).

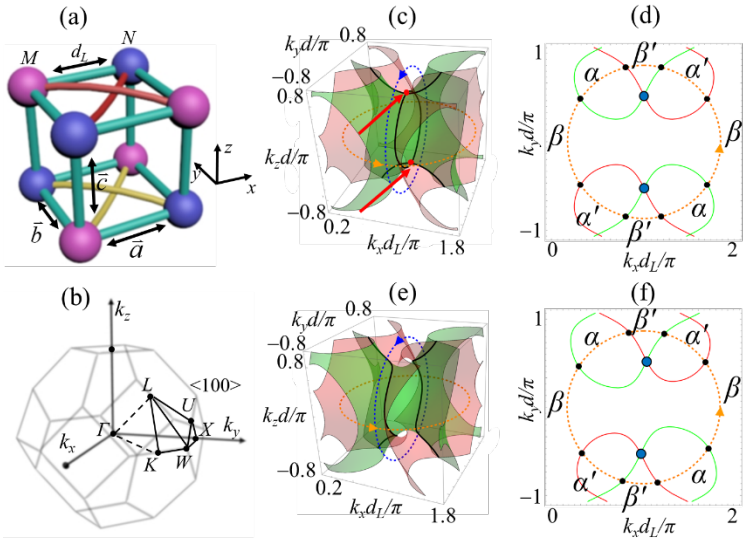

Fig. 4. Proposal of an fcc lattice model with non-reciprocal hoppings. (a) fcc lattice with two sites M (blue balls) and N (pink balls). The interspace distance between M and N is d_L, and $\vec{a}$, $\vec{b}$ and $\vec{c}$ are bond vectors. The hopping on dark green bonds is non-reciprocal ($M\rightarrow N$: t_1, $N\rightarrow M$: $-t_1$). The hopping on the same lattice sites in different directions (in $\vec{a}+\vec{b}$ and $\vec{a}-\vec{b}$) have opposite signs (hopping on yellow bonds: t_2, hopping on red bonds: $-t_2$). (b) First Brillouin zone of the fcc lattice. (c, e) ESs (red and green surfaces) and NILs (black lines) for $E_0=0$ and $E_0\neq 0$ in Eq. (6). (c) has a chain of NILs, which is symmetric with respect to <100> plane. The intersecting points on the chain are labelled with red arrows. (d, f) Cross section of the plane $k_z=0$ (where the orange loop locates) for (c) and (d), respectively. The topological charge on the loop is conserved even though the mirror symmetries are broken.